Supporting information

Strategic tuning of excited-state properties of electroluminescent materials with enhanced hot exciton mixing

Jayaraman Jayabharathi*, Venugopal Thanikachalam, Ramaiyan Ramya, Sekar Panimozhi

Department of Chemistry, Annamalai University, Annamalai nagar, Tamilnadu- 608 002, India

* Address for correspondence

Dr. J. Jayabharathi
Professor of Chemistry
Department of Chemistry
Annamalai University
Annamalai nagar 608 002
Tamilnadu, India.
Tel: +91 9443940735
E-mail: jtchalam2005@yahoo.co.in

Contents

Scheme S1. Effect of TADF and HLCT on 100 % exciton utilization efficiency (η_s).

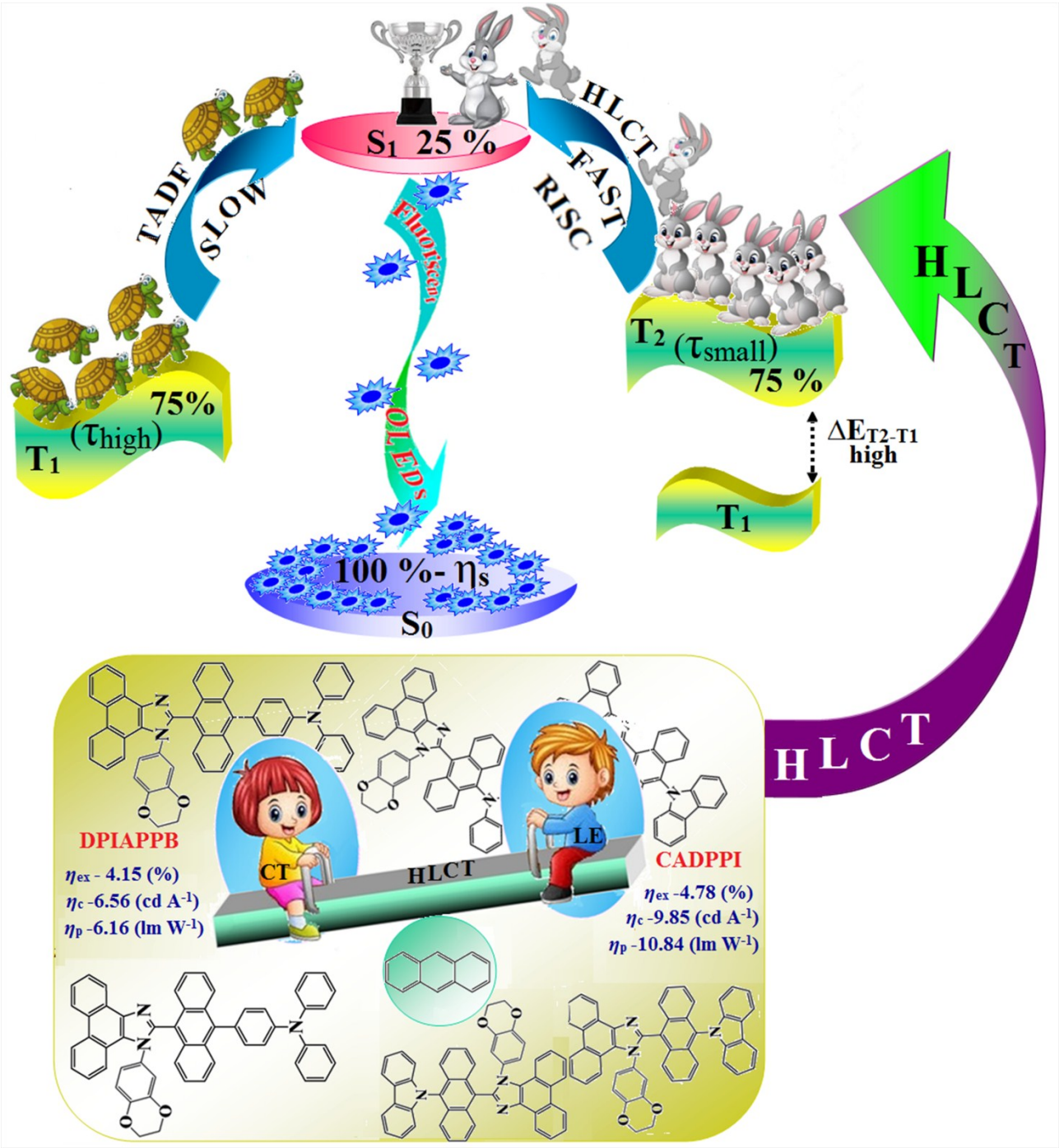

Figure S1. Potential energy surface scan (PES) diagram of (a) CADPPI and DPIAPPB; (b) Potential energy scan (PES) of excited states of (b) CADPPI and (c) DPIAPPB with increasing solvent polarity

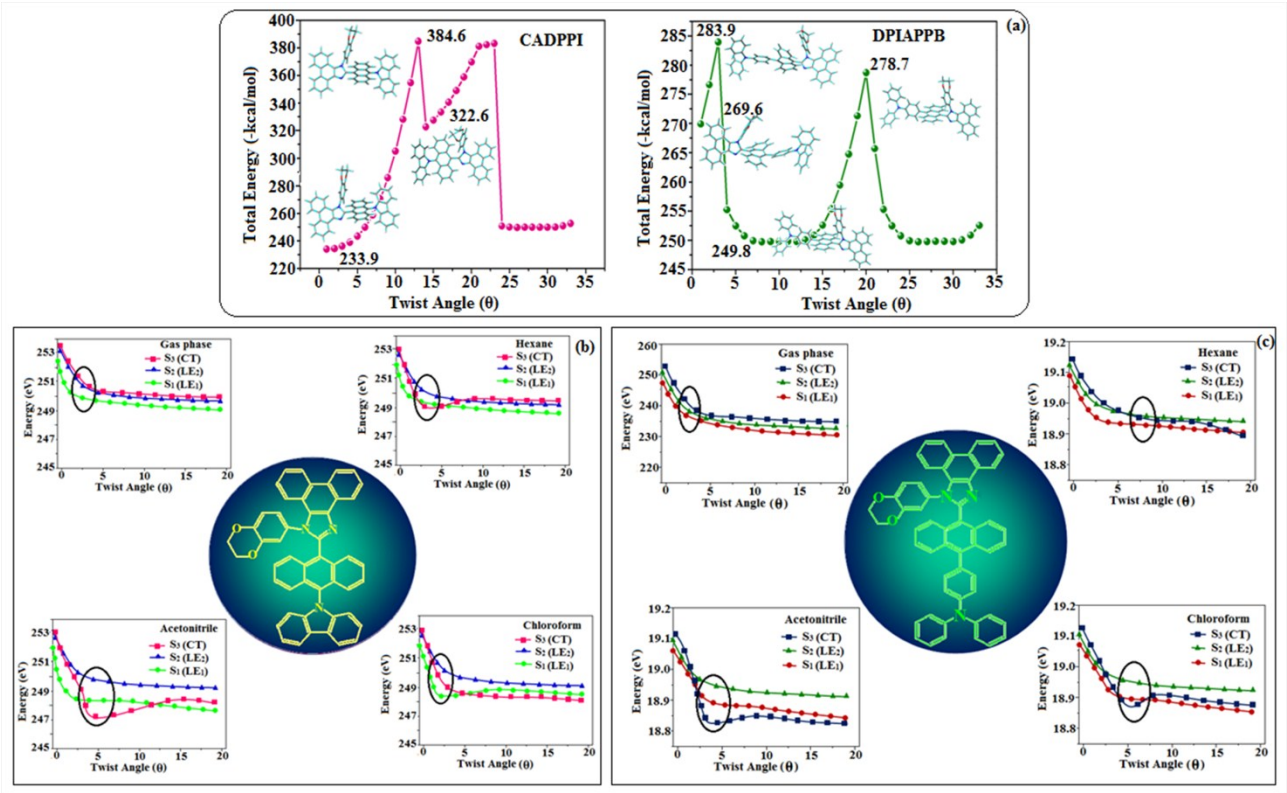

Figure S2. (a) TGA (inset: DSC) graph and (b) Lifetime spectra of CADPPI and DPIAPPB

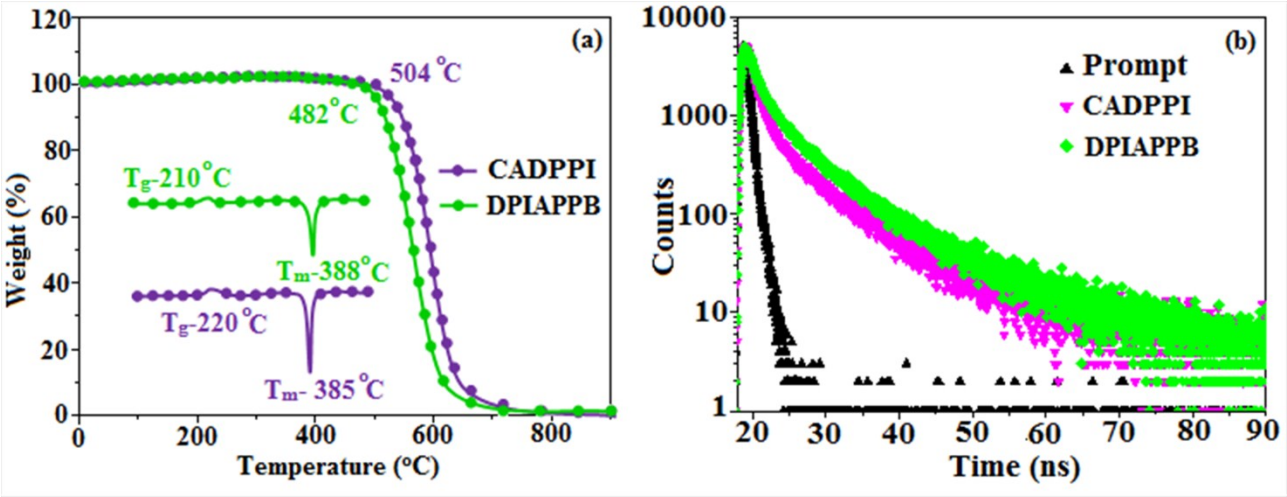

Figure S3. MEP, optimized geometry and HOMO and LUMO of CADPPI and DPIAPPB

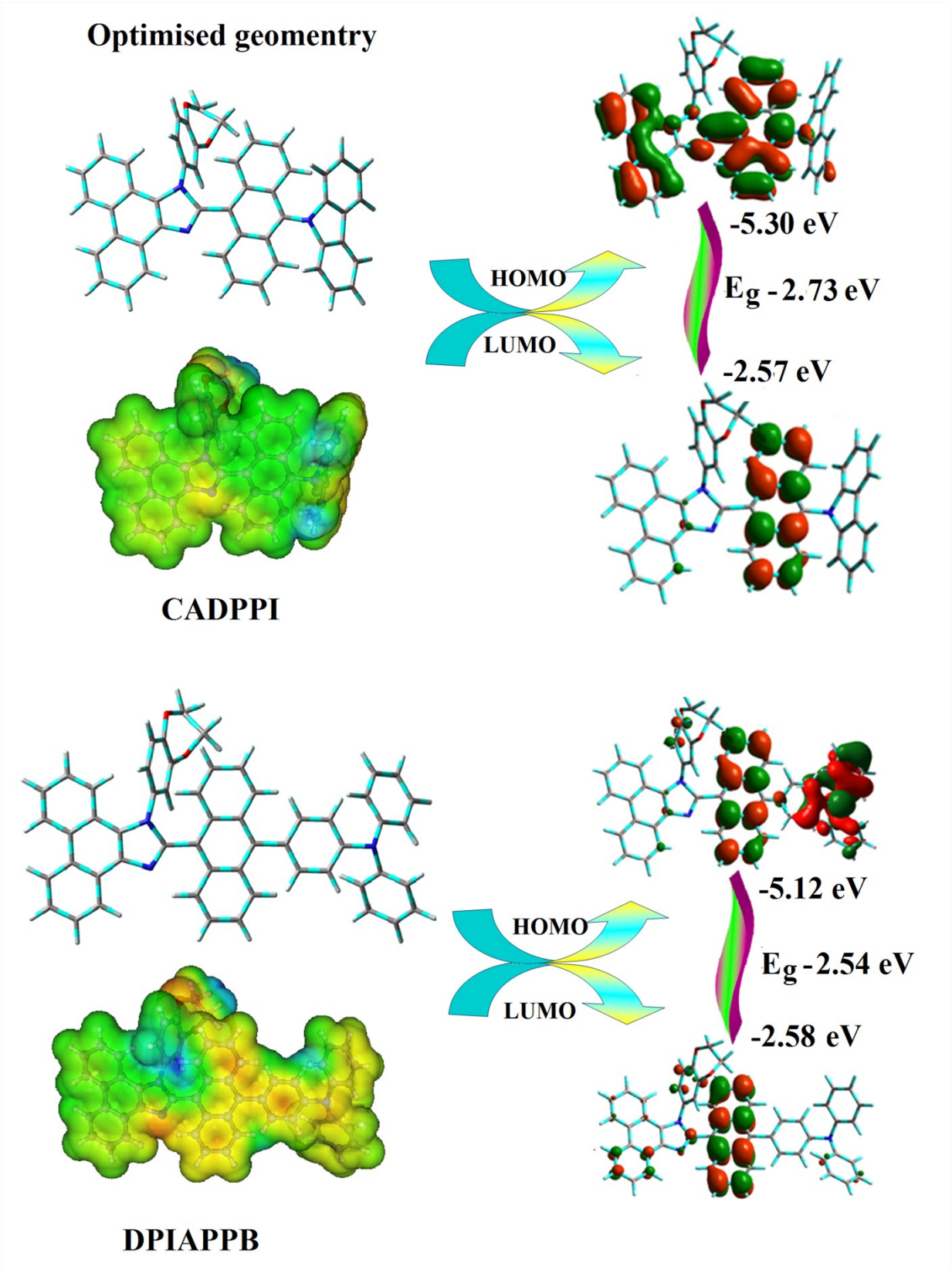

SI-II. Solvantochromism for HLCT character- Lippert-Mataga plot

The solvatochromic effect using Lippert-Mataga plot has been displayed in Figure 2. When solvent polarity was increased the blue emitters exhibit a larger red shift which supports charge transfer in these molecules. The properties of ground state (S_0) and the lowest singlet excited state (S_1) can be better understood through solvatochromic experiment. We use the Lippert-Mataga equation to explore the influence of solvent environment on the optical property of our materails, the model can describes the interaction between the solvent and the dipole moment of solute:

$$hc(\tilde{\upsilon}_a - \tilde{\upsilon}_f) = hc(hc\tilde{\upsilon}_a^{vac} - hc\tilde{\upsilon}_f^{vac}) + 2(\mu_e - \mu_g)^2 / a_o^3 f(\varepsilon, n)$$

where f is the orientational polarizability of the solvent, $\tilde{\upsilon}_a - \tilde{\upsilon}_f$ corresponds to the Stokes shifts when f is zero, μ_e is the excited state dipole moment, μ_g is the ground-state dipole moment; a is the solvent cavity (Onsager) radius, derived from the Avogadro number (N), molecular weight (M), and density (d = 1.0 g cm^{-3}); ε and n are the solvent dielectric and the solvent refractive index, respectively; $f(\varepsilon, n)$ and a can be calculated respectively as follows:

$$f(\varepsilon, n) = [(\varepsilon - 1/2\varepsilon + 1) - \tfrac{1}{2}(n^2 - 1/2n^2 + 1)]$$

$$a = (3M/4N\pi d)^{1/3}$$

The relationships between stokes shift and solvent polarity are presented in Figure 2, The ground state dipole (μ_g) of blue emitting materials, DPIAPPB and CADPPI could be estimated from density functional theory (DFT) calculation as, 4.67 and 8.5 D, respectively which is attributed by local exciton (LE) transition and μ_e in high polar solvents is 23.9 and 24.1 D, respectively [57]. The non-linear correlation of Stokes shift *Vs* solvent polarity function reveal that there is transformation of fitted line between ethyl ether and methylene chloride: non-linear correlation supports the presence of both locally excited state (LE) and charge transfer excited state (CT).

Figure S4. Solvatochromic emission spectra of a) CADPPI and b) DPIAPPB

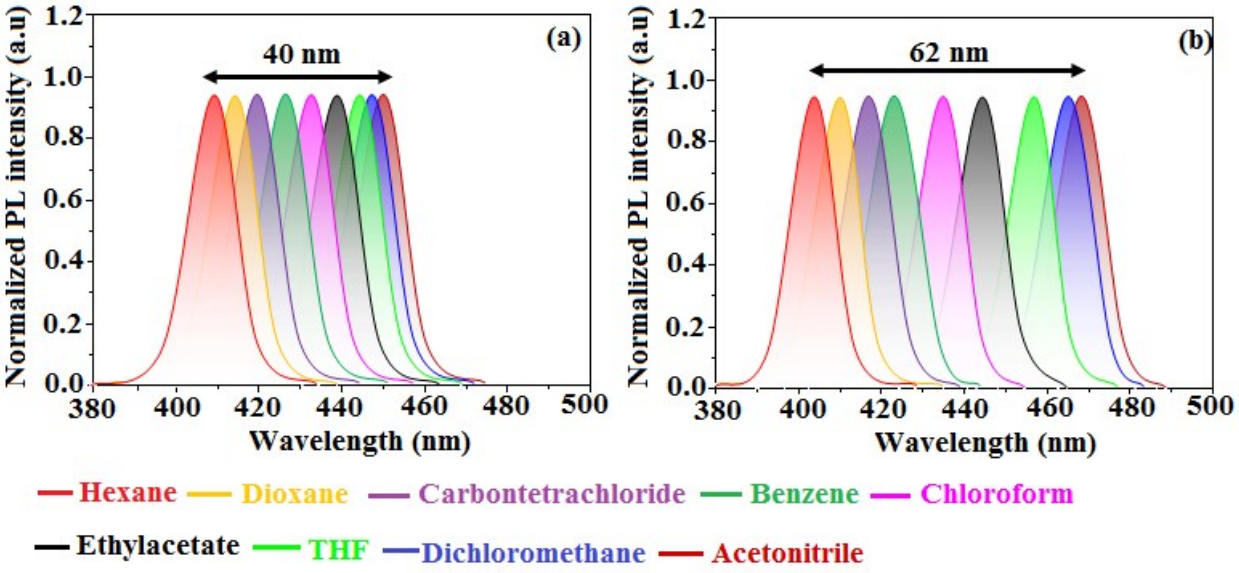

Figure S5. Normalized absorption spectra of a) CADPPI and b) DPIAPPB

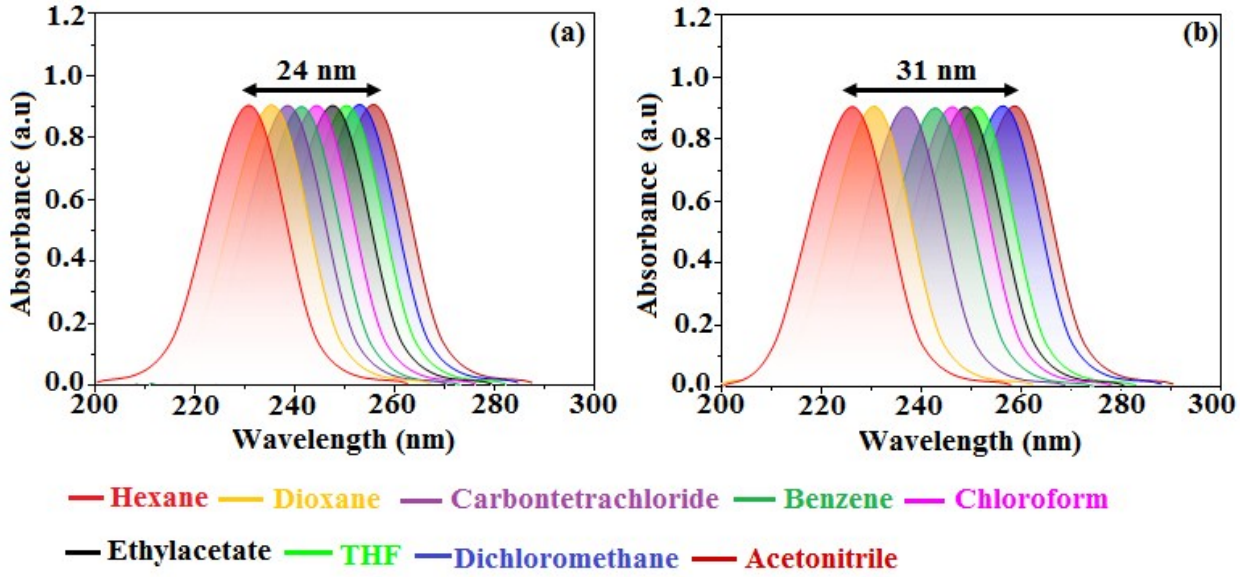

SI–III: Charge–Transfer intexes

The hole–particle pair interactions have been related to the distance covered during the excitations one possible descriptor Δr intex could be used to calculate the average distance which is weighted in function of the excitation coefficients.

$$\Delta r = \frac{\Sigma_{ia} k_{ia}^2 \left| \langle \varphi_a | r | \varphi_a \rangle - \langle \varphi_i | r | \varphi_i \rangle \right|}{\Sigma_{ia} K_{ia}^2} \quad \text{…….. (S1)}$$

where $\left| \langle \varphi_i | r | \varphi_i \rangle \right|$ is the norm of the orbital centroid [1–4]. Δr–index will be expressed in Å.

The density variation associated to the electronic transition is given by

$$\Delta\rho(r) = \rho_{EX}(r) - \rho_{GS}(r) \quad \text{..... (S2)}$$

where $\rho_{GS}(r)$ and $\rho_{EX}(r)$ are the electronic densities of to the ground and excited states, respectively. Two functions, $\rho_+(r)$ and $\rho_-(r)$, corresponds to the points in space where an increment or a depletion of the density upon absorption is produced and they can be defined as follows:

$$\rho_+(r) = \begin{Bmatrix} \Delta\rho(r) & if\ \Delta\rho(r) > 0 \\ 0 & if\ \Delta\rho(r) < 0 \end{Bmatrix} \quad \text{..... (S3)}$$

$$\rho_-(r) = \begin{Bmatrix} \Delta\rho(r) & if\ \Delta\rho(r) < 0 \\ 0 & if\ \Delta\rho(r) > 0 \end{Bmatrix} \quad \text{..... (S4)}$$

The barycenters of the spatial regions R_+ and R_- are related with $\rho_+(r)$ and $\rho_-(r)$ and are shown as

$$R_+ = \frac{\int r\rho_+(r)dr}{\int \rho_+(r)dr} = (x_+, y_+, z_+) \quad \text{..... (S5)}$$

$$R_- = \frac{\int r\rho_-(r)dr}{\int \rho_-(r)dr} = (x_-, y_-, z_-) \quad \text{..... (S6)}$$

The spatial distance (D_{CT}) between the two barycenters R_+ and R_- of density distributions can thus be used to measure the CT excitation length

$$D_{CT} = \left|R_+ - R_-\right| \quad \text{(S7)}$$

The transferred charge (q_{CT}) can be obtained by integrating over all space $\rho_+(\rho_-)$,. Variation in dipole moment between the ground and the excited states (μ_{CT}) can be computed by the following relation:

$$\|\mu_{CT}\| = D_{CT}\int \rho_+(r)dr = D_{CT}\int \rho_-(r)dr \quad \text{(S8)}$$

$$= D_{CT}q_{CT} \quad \text{(S9)}$$

The difference between the dipole moments $\|\mu_{CT}\|$ have been computed for the ground and the excited states $\Delta\mu_{ES-GS}$. The two centroids of charges (C^+/C^-) associated to the positive and negative density regions are calculated as follows. First the root–mean–square deviations along the three axis (σ_{aj}, j = x, y, z; a = + or –) are computed as

$$\sigma_{a,j} = \sqrt{\frac{\sum_i \rho_a(r_i)(j_i - j_a)^2}{\sum_i \rho_a(r_i)}} \quad \text{(S10)}$$

The two centroids (C_+ and C_-) are defined as

$$C_+(r) = A_+ e\left(-\frac{(x-x_+)^2}{2\sigma_{+x}^2} - \frac{(y-y_+)^2}{2\sigma_{+y}^2} - \frac{(z-z_+)^2}{2\sigma_{+z}^2}\right) \quad \text{(S11)}$$

$$C_-(r) = A_- e\left(-\frac{(x-x_-)^2}{2\sigma_{-x}^2} - \frac{(y-y_-)^2}{2\sigma_{-y}^2} - \frac{(z-z_-)^2}{2\sigma_{-z}^2}\right) \quad \text{(S12)}$$

The normalization factors (A+ and A_) are used to impose the integrated charge on the centroid to be equal to the corresponding density change integrated in the whole space:

$$A_{+} = \frac{\int \rho_{+}(r)dr}{\int e\left(-\frac{(x-x_{-})^2}{2\sigma_{+x}^2} - \frac{(y-y_{-})^2}{2\sigma_{+y}^2} - \frac{(z-z_{-})^2}{2\sigma_{+z}^2}\right)dr} \quad \text{..... (S13)}$$

$$A_{-} = \frac{\int \rho_{-}(r)dr}{\int e\left(-\frac{(x-x_{-})^2}{2\sigma_{-x}^2} - \frac{(y-y_{-})^2}{2\sigma_{-y}^2} - \frac{(z-z_{-})^2}{2\sigma_{-z}^2}\right)dr} \quad \text{..... (S14)}$$

H index is defined as half of the sum of the centroids axis along the D–A direction, if the D–A direction is along the X axis, H is defined by the relation:

$$H = \frac{\sigma_{+x} + \sigma_{-x}}{2} \quad \text{..... (S15)}$$

The centroid along X axis is expected. The t intex represents the difference between D_{CT} and H:

$$t = D_{CT} - H \quad \text{..... (S16)}$$

The integral of hole (h^+) and electron (e^-) of CADPPI is less than DPIAPPI with transition density. The integral overlap of hole-electron (Figure S9 CADPPI; Figure S10 DPIAPPI) distribution (S) is a measure of spatial separation of hole and electron. The integral overlap (S) of hole and electron and distance (D) between centroids of hole and electron confirmed the existence of LE and CT states. Compared to parent compounds, CADPPI and DPIAPPI has small D and high S value, however, The small D and high S of DPIAPPI on comparison to CADPPI indicates charge transfer is higher in percentage for DPIAPPI. The variation of dipolemoment with respect to S_0 is outputted which is directly evaluated based on the position of centroid of hole and electron. RMSD of hole or electron characterizes their distribution breadth: RMSD of both electron and hole in CADPPI is higher in X direction, indicates electron and hole distribution is much broader in X direction whereas RMSD of electron in DPIAPPI is smaller and hole is higher than TPNCN-Cz. The H intex (half sum of the axis of anistropic density variation distribution) measures the spread of positive and negative regions related to CT. The CT intex, *i.e., t* index (D_{CT} - H intex) is another measure of separation of hole-electron (equations S15 and S16). The D_{CT} of CADPPI and DPIAPPI is calculated to be 0.19 and 0.16, respectively (Figure S11). For both CADPPI and TPNCN-TPA, *t* is negative in all directions which reveal that the overlap of hole and electron is very severe (Figure S11) and eign value is greater than 0.96 which supports the hybridization and described in terms of dominant excitation pair in term of 94% of transition. This is further evidenced by Δr intex (equation S1) which is average of hole -electron distance ($d_{h^+ - e^-}$) upon excitation which shows the nature of excitation type, LE or CT: valence excitation (LE) is related to short distance ($< d_{h^+ - e^-}$) while the larger distance ($> d_{h^+ - e^-}$) is related to CT excitation. The triplet exciton is transformed to singlet exciton in DPIAPPI and CADPPI through RISC process with high energy excited state (hot CT channel) [1] which is beneficial for triplet exciton conversion in electroluminescence process without any delayed fluorescence. The CT excitons are formed with weak binding energy (E_b) on higher

excited states, [2] as a result; the exciton utilization (η_s) can be harvested in DPIAPPI and CADPPI like phosphorescent materials. The quasi-equivalent hybridized materials exhibit excellent device performances due to fine modulation in excited states: enhanced LE component and hybridization between LE and CT components results high η_{PL} and high η_s. The coexisting LE/CT composition in DPIAPPI and CADPPI harvested high η_{PL} and high η_s and enhanced OLEDs efficiencies.

Figure S6. Natural transition orbital pairs with (HONTOs and LUNTOs) transition character analysis for singlet states (S_1-S_5) and triplet states (T_1-T_5) of CADPPI [*f*-oscillator strength and % weights of hole-particle].

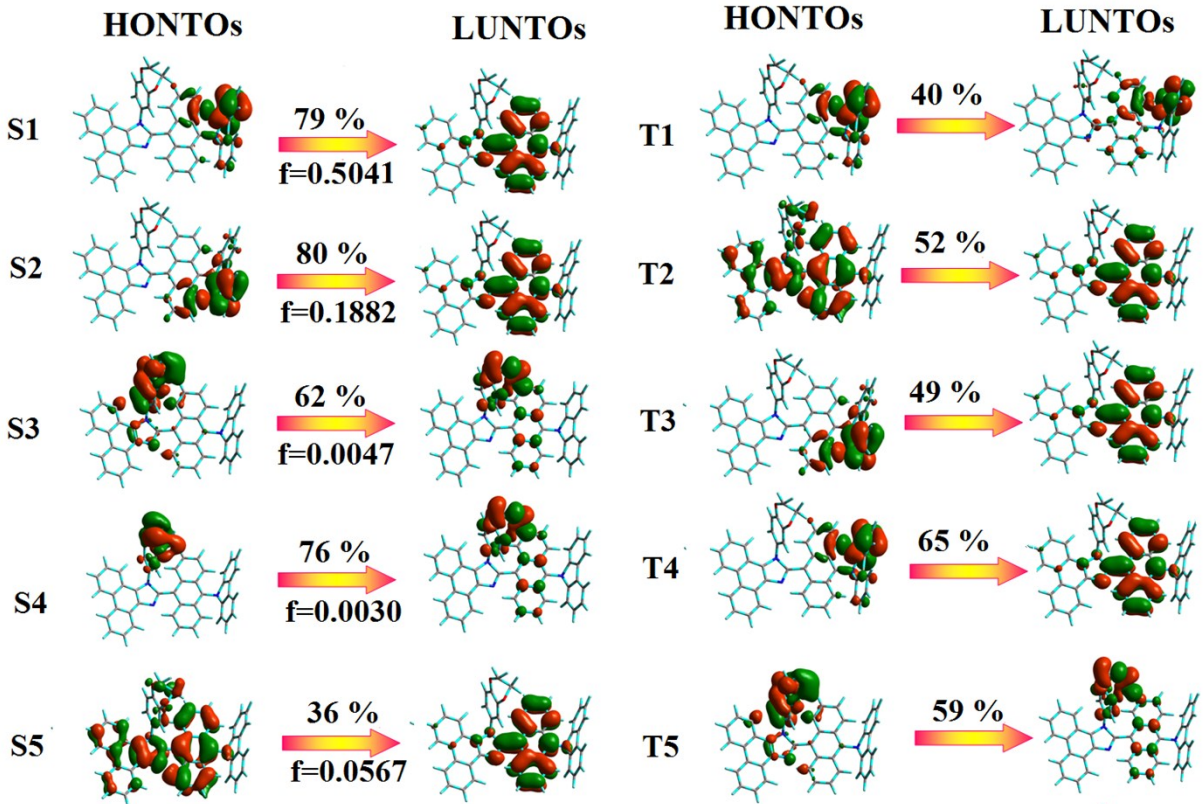

Figure S7. Natural transition orbital pairs (HONTOs & LUNTOs) with transition character analysis for singlet states (S_1-S_5) and triplet states (T_1-T_5) of DPIAPPB [*f*-oscillator strength and % weights of hole-particle].

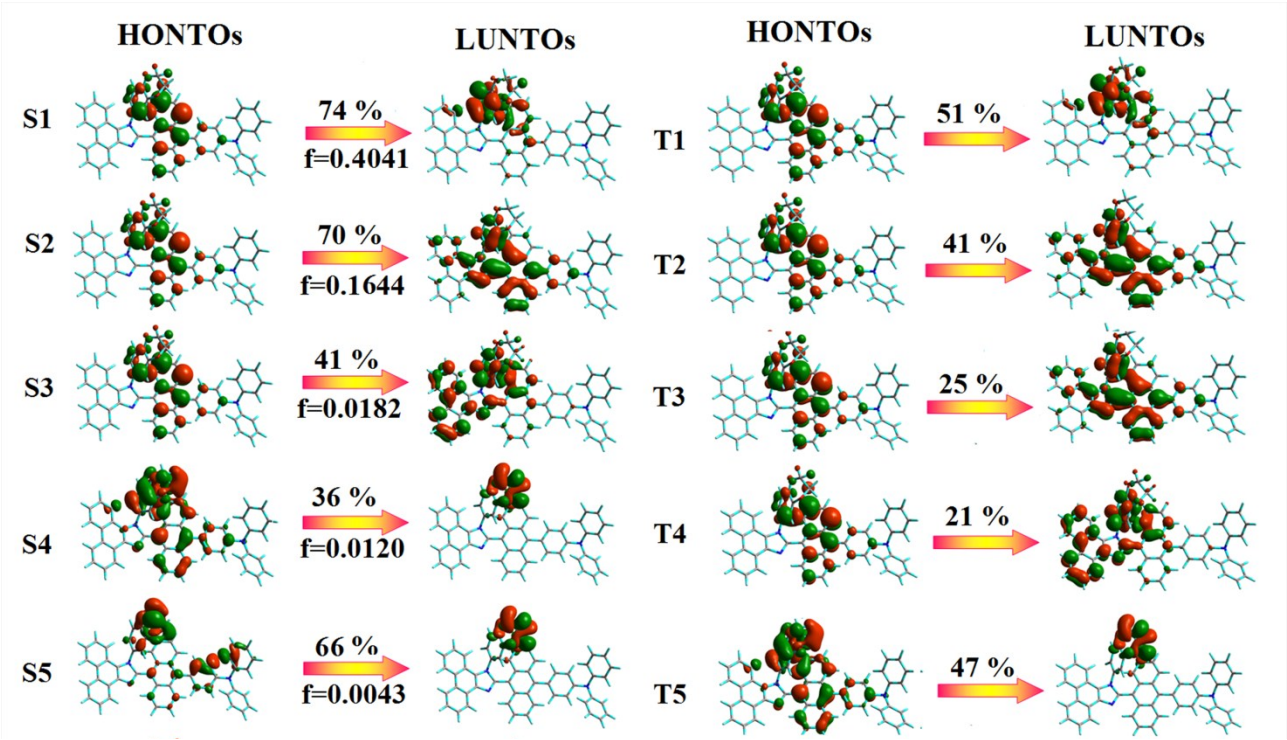

Figure S8. Frontier molecular orbitals of CADPPI and DPIAPPB at 50° and 180° twist angles

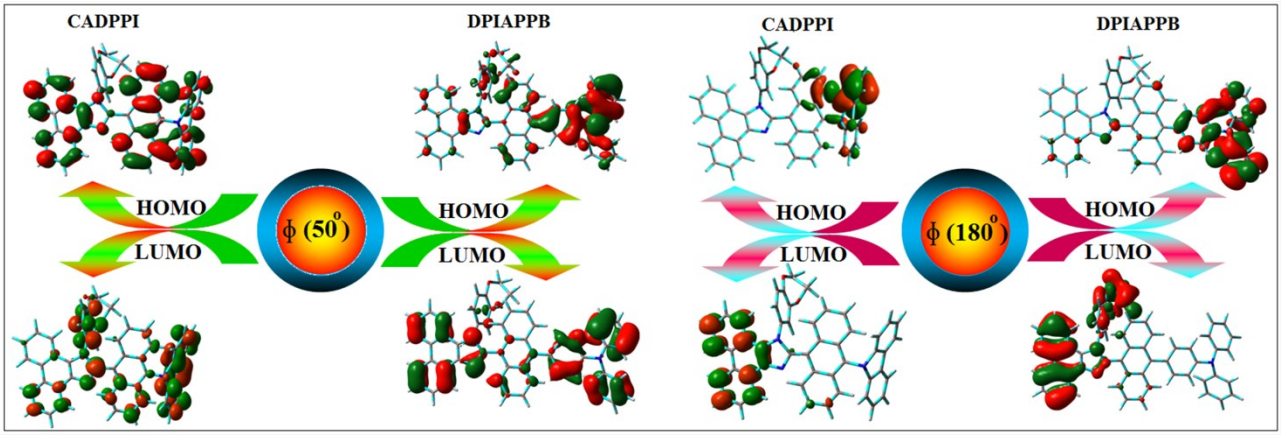

Figure S9. Hole and particle distribution [S_1–S_5 states: ●-green increasing electron density and ● blue decreasing electron density and Computed contour plots of transition density matrices (TDM) of CADPPI for [S_1–S_5 states: density=transition=n /IOp(6/8=3)].

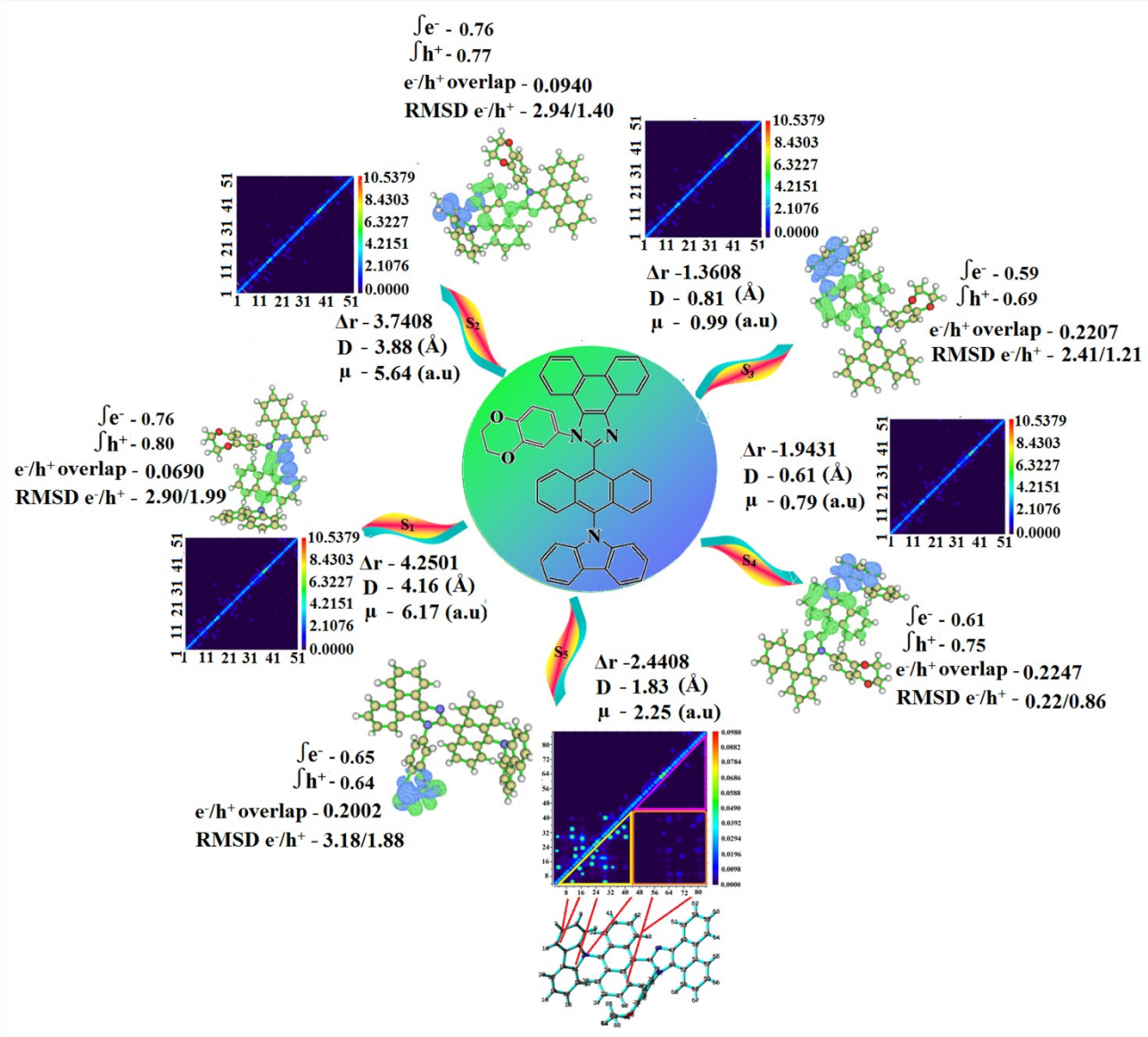

Figure S10. Hole and particle distribution [S_1–S_5 states: ● -green increasing electron density and ● - blue decreasing electron density and Computed contour plots of transition density matrices (TDM) of DPIAPPB for [S_1–S_5 states: density=transition=n /IOp(6/8=3)].

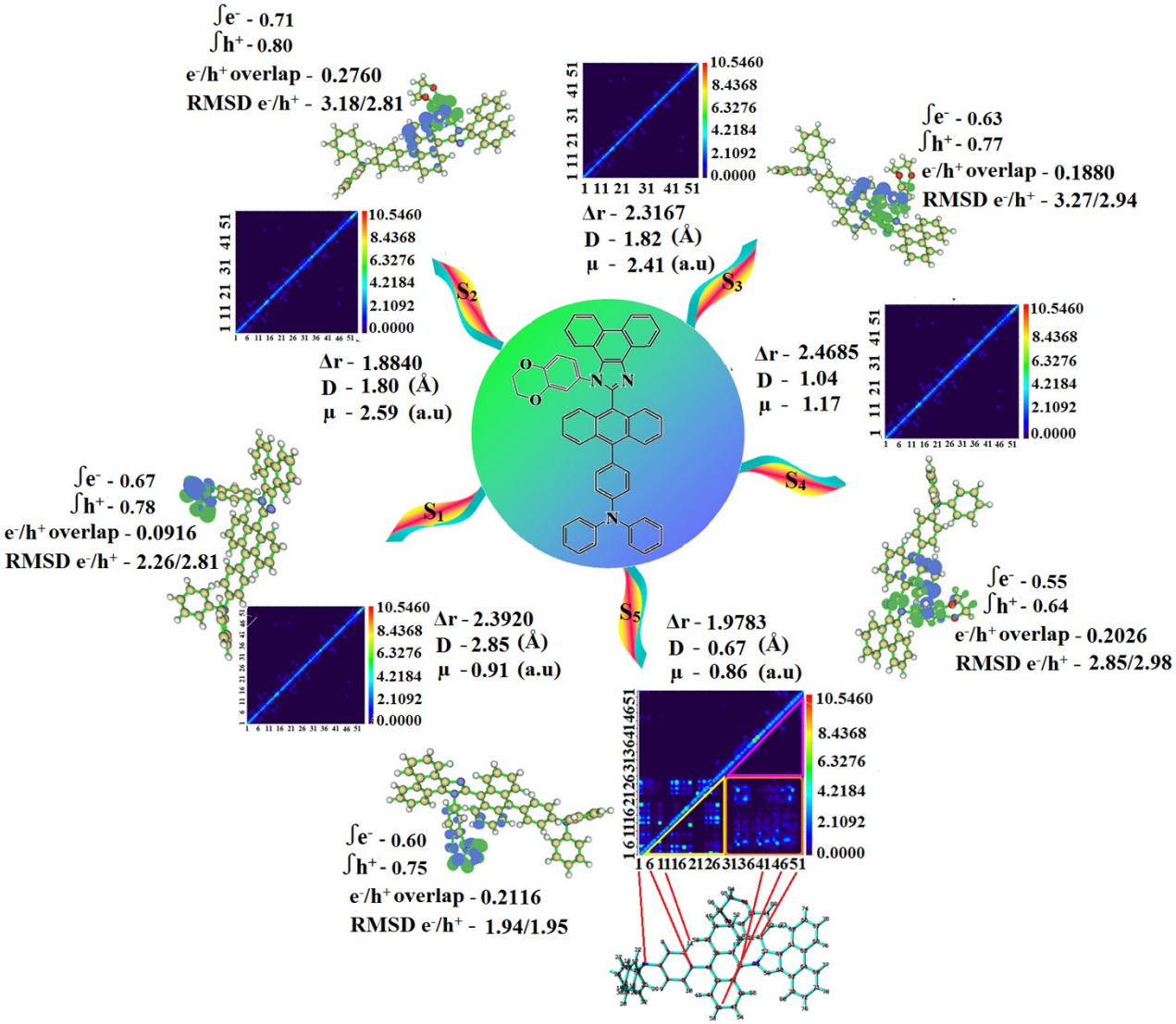

Figure S11. Computed difference in total density for ground and excited states [$\Delta\rho\ (r)=\rho_{Ex}\ (r)-\rho_{Gs}\ (r)$; isosurface for CADPPI, DPIAPPB (0.0000006 a.u); graphical representation of D_{CT} and centroid of charges [C+(r) / C-(r); isosurface for CADPPI, (0. 29 a.u) and for DPIAPPB (0.1 a.u)]

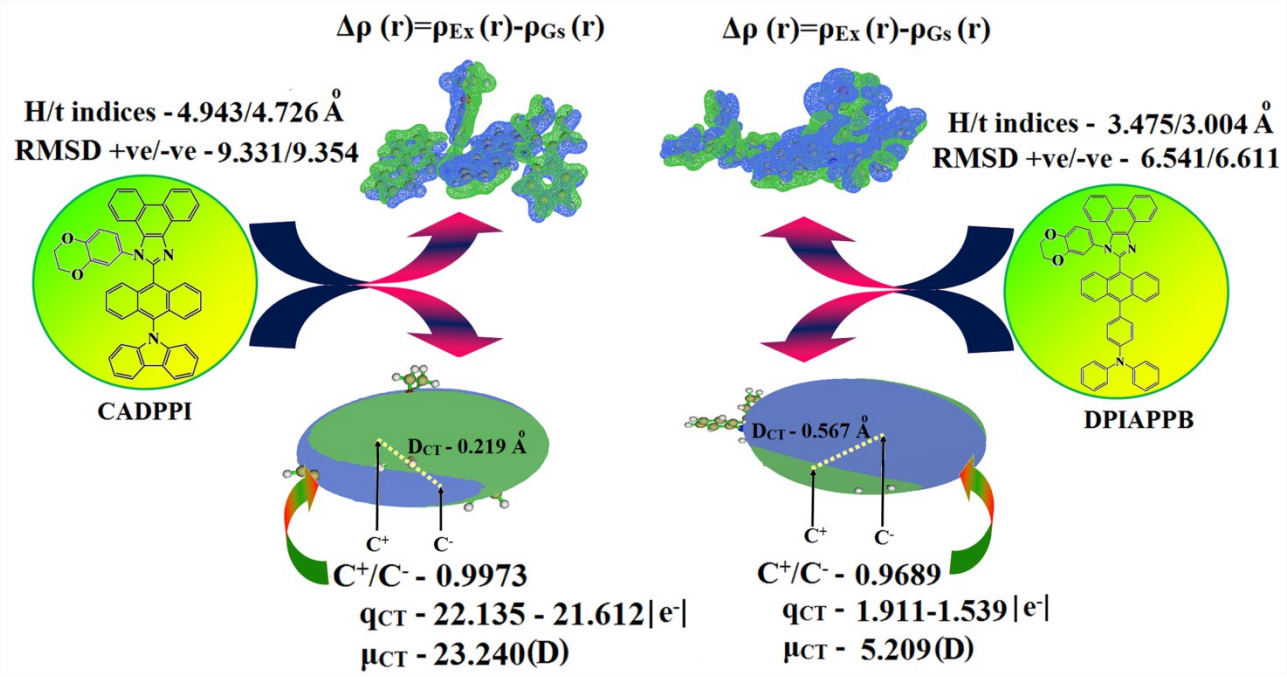

Figure S12. Structural formula for the emitters displayed in Table 3.

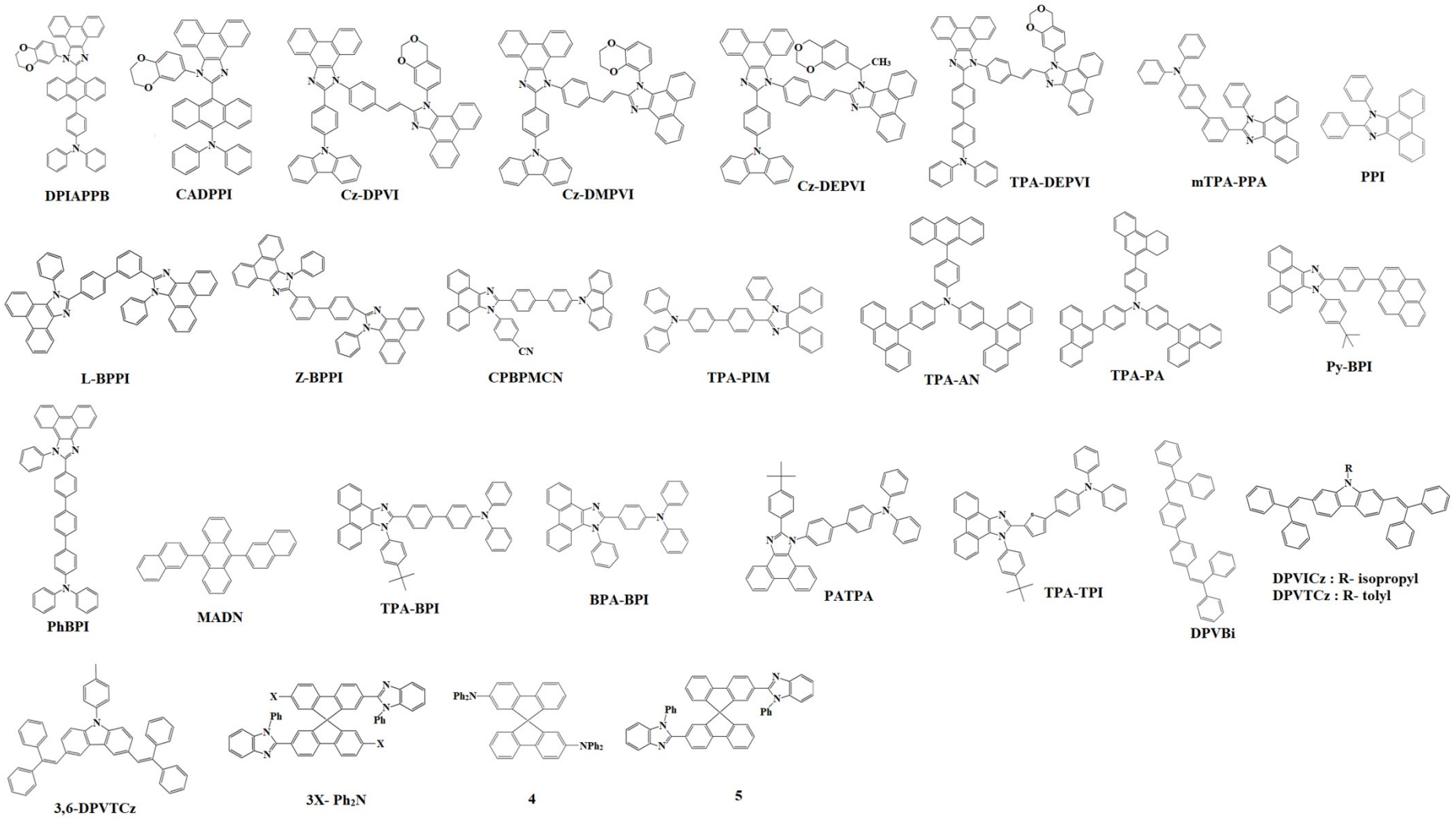

Reference

[1] (a) M. Segal, M. Singh, K. Rivoir, S. Difley, T. V. Voorhis and M. A. Baldo, *Nat. Mater.,* 2007, **6**, 374; (b) W. Barford, *Phys. Rev. B.,* 2004, **70**, 205204.

[2] W. Jiang and L. Duan Qiao, *J. Org. Lett.,* 2011, **13**, 3146.